Article

Prediction of the Potentially Suitable Areas of Sesame in China Under Climate Change Scenarios Using MaxEnt Model

Guoqiang Li [1,2], Xue Wang [1,3], Jie Zhang [1,2], Feng Hu [1,2], Hecang Zang [1,2], Tongmei Gao [4], Youjun Li [3,*] and Ming Huang [3,*]

1   Institute of Agricultural Information Technology, Henan Academy of Agricultural Sciences, Zhengzhou 450008, China; gqli@hnagri.org.cn (G.L.); xuewang@stu.haust.edu.cn (X.W.)
2   Key Laboratory of Huang-Huai-Hai Smart Agricultural Technology, Ministry of Agriculture and Rural Areas, Zhengzhou 450008, China
3   College of Agriculture, Henan University of Science and Technology, Luoyang 471023, China
4   Henan Sesame Research Center, Henan Academy of Agricultural Sciences, Zhengzhou 450008, China
*   Correspondence: lyj@haust.edu.cn (Y.L.); huangming@haust.edu.cn (M.H.)

Abstract: Sesame (*Sesamum indicum* L., flora of China) is an essential oil crop in China, but its growth and development are affected by climate change. To cope with the impacts of climate change on sesame cultivation, we used the Maximum Entropy (MaxEnt) model to analyze the bioclimatic variables of climate suitability of sesame in China and predicted the suitable area and trend of sesame in China under current and future climate scenarios. The results showed that the MaxEnt model prediction was excellent. The most crucial bioclimatic variable influencing the distribution of sesame was max temperature in the warmest month, followed by annual mean temperature, annual precipitation, mean diurnal range, and precipitation of the driest month. Under the current climate scenario, the suitable areas of sesame were widely distributed in China, from south (Hainan) to north (Heilongjiang) and from east (Yellow Sea) to west (Tibet). The area of highly suitable areas was 64.51×10^4 km^2, accounting for 6.69% of the total land area in China, and was primarily located in mainly located in southern central Henan, eastern central Hubei, northern central Anhui, northern central Jiangxi, and eastern central Hunan. The area of moderately suitable areas and lowly suitable areas accounted for 17.45% and 25.82%, respectively. Compared with the current climate scenario, the area of highly and lowly suitable areas under future climate scenarios increased by 0.10–11.48% and 0.08–8.67%, while the area of moderately suitable areas decreased by 0.31–23.03%. In addition, the increased highly suitable areas were mainly distributed in northern Henan. The decreased moderately suitable areas were mainly distributed in Heilongjiang, Jilin, and Liaoning. This work is practically significant for optimizing the regional layout of sesame cultivation in response to future climate conditions.

Keywords: sesame (*Sesamum indicum* L.); climate change; climatic suitability; maximum entropy (MaxEnt) model

1. Introduction

The global average temperature has risen by 0.9 °C since the 19th century and is expected to increase further by 0.3 °C to 4.8 °C [1,2]. Water resources are becoming increasingly scarce and are expected to decrease further [3]. Temperature and precipitation are key factors determining crop growth and development and have a clear relationship with the spatial distribution of crops [4,5]. High temperatures result in the falling of crops at the reproductive stage. Water shortage can delay plant development and result in a decrease in economic yield. Crop suitability determines crop planting distribution in a given region [6,7]. Therefore, assessing the effects of climate change on crop suitability helps further optimize crop-growing areas.

Simulation modeling is the best tool for assessing climatic suitability. Various species distribution models (SDMs) are widely used to predict how the potential distribution areas of crop species response to the projected climate change [8]. SDMs can simulate the potential distribution of species in related areas by associating the observed distribution records of species with environmental factors [9–11]. These models include the dynamic simulation model (BIOCLIM and CLIMEX), generalized linear model (GLM), generalized additive model (GAM), maximum entropy model (MaxEnt), and random forest (RF) [12,13]. In recent years, the MaxEnt model has been utilized to forecast the geographic distributions of species using environmental information [10,14]. Huang et al. [15] utilized the MaxEnt model and ArcGIS (version 10.8) software to map the distribution of suitable areas of invasive weeds in Asia under climate change conditions. Parthapratim et al. [16] identified the key bioclimatic variables and assessed how climate change affects the habitat suitability and morphological traits of *Begonia aborensis* Dunn (flora of China) in Northeastern India. Zhang et al. [17] analyzed the ecological distribution and patterns of grasshopper occurrences using the MaxEnt model. Lu et al. [18] assessed the current climatic suitability for soybeans (Glycine max (L.) Merr, flora of China and projected future climatic suitability trends under various climate change scenarios. Wang et al. [19] predicted the distribution range of *Leonurus japonicus* Houtt (flora of China) in China under climate change, providing the scientific basis for conservation and utilization. Thus, the MaxEnt model can be effectively used to evaluate the climatic suitability of sesame in China.

Sesame (*Sesamum indicum* L.) is one of the oldest and most important oil crops and is widely cultivated across the world, particularly in rainy areas [20]. The sesame planting areas in China rank fourth globally, accounting for about 10% of the global planting area. To improve sesame cultivation and cope with climate change, assessing the effects of climate change on the climatic suitability of sesame at the national scale is valuable. Abebe et al. [21] investigated the impact of climate change on sesame yield in North Ethiopia using the autoregressive distributed lag time series model. Baath et al. [22] developed crop models using estimated temperature limits to simulate the sesame management strategies under various climate scenarios. Wang et al. [23] assessed the climatic suitability of sesame in China's main sesame planting areas from 1978 to 2019 based on fuzzy mathematics. The SSPs (shared socioeconomic pathway) are a set of integrated scenarios that outline socioeconomic development and emissions, serving as key input parameters for climate change prediction models in the 21st century [24]. SSP126 represents a low greenhouse gases (GHG) concentration under government intervention with radiative forcing at 2.6 W/m^2 after 2100; SSP245 represents a scenario with radiative forcing at 4.5 W/m^2 after 2100; SSP370 represents a scenario with radiative forcing at 7.0 W/m^2 after 2100, and SSP585 is a scenario of high concentrations of GHG emissions without climate change policy intervention [25]. These scenarios are designed to outline future changes in population, socioeconomic factors, scientific and technological advancements, energy consumption, and the emissions of GHG [26]. However, there have been no reports on evaluating the distribution and spatial patterns of sesame in China under various climate scenarios using the MaxEnt model.

In this study, the key bioclimatic variables affecting sesame growth were analyzed by the jackknife method. The MaxEnt model combined with ArcGIS software was used to predict the potentially suitable areas of sesame in China under the current scenario from 1970 to 2000 and future scenarios (SSP126, SSP245, SSP370, and SSP585) in different periods (2021–2040, 2041–2060, 2061–2080, and 2081–2100). The objectives of this study were as follows: (1) to reveal the bioclimatic variables affecting the suitability for sesame cultivation and analyze the relationship between the predicted suitable areas and the main bioclimatic variables; (2) to forecast the suitable areas of sesame under current and future climate scenarios and divide them into different suitability grades; and (3) to predict the suitable areas and then compare the change trends of sesame under the climate periods in 2021–2040, 2041–2060, 2061–2080, and 2081–2100. This study will offer a scientific foundation for sesame cultivation in China.

2. Materials and Methods

2.1. Occurrence Data of Sesame

The distribution points of sesame were obtained from the Global Biodiversity Information Facility (https://www.gbif.org/, accessed on 1 February 2024), the China Virtual Herbarium (https://www.cvh.ac.cn/, accessed on 3 February 2024), and the China National Specimen Information Infrastructure (https://www.nsii.org.cn, accessed on 6 February 2024). We removed the records with geo-referencing and data entry errors using the R (version 4.2.2) package Coordinate Cleaner. A total of 234 sesame distribution points were obtained (Figure 1). Then, we edited the latitude and longitude of the distribution points in Excel. The China map used as the base map in ArcGIS software was downloaded from the Data Center for Resource and Environmental Sciences, Chinese Academy of Sciences (https://www.resdc.cn/, accessed on 8 February 2024).
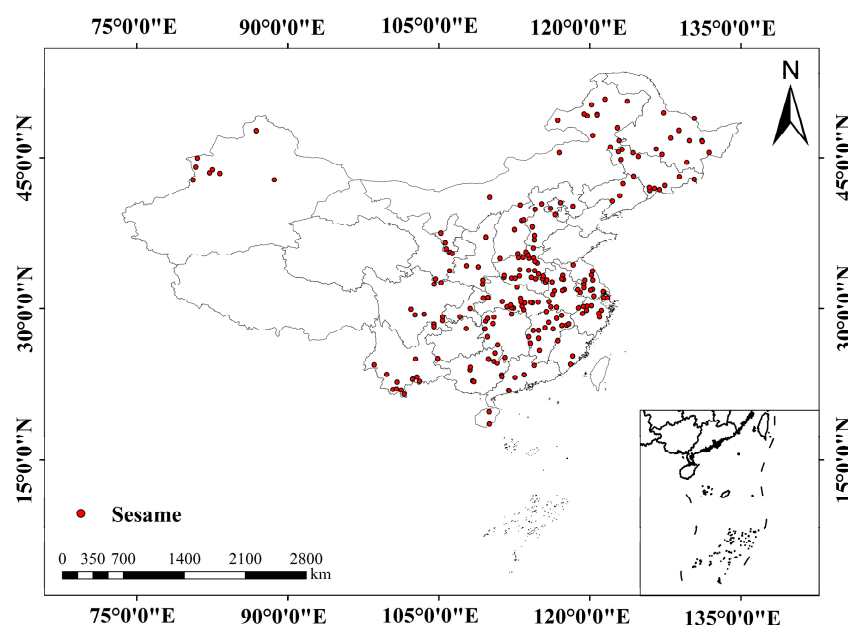

Figure 1. Distribution points of sesame in China.

2.2. Selection of Bioclimatic Variables

We downloaded bioclimatic variables for the current period (1970–2000) and four future periods (2021–2040, 2041–2060, 2061–2080, 2081–2100) used in the study from the WorldClim database (http://www.wordclim.org, accessed on 5 February 2024). These bioclimatic variables include 19 variables (Bio1–Bio19, Table 1) with a spatial resolution of 2.5 arc-minutes. The future bioclimatic variables are derived from the BCC-CSM2-MR climate system model, which was developed by the China National Climate Center.

Many bioclimatic variables tend to increase the dimensionality of the ecological space due to high collinearity among bioclimatic variables [27], leading to unfavorable model predictions. Thus, it is essential to screen the bioclimatic variables for this study. Firstly, the jackknife method was employed to evaluate the contribution percentage of 19 bioclimatic variables, and the variables with a contribution rate of less than 1% were removed. Secondly, the correlation coefficient was conducted by the ENMTools tool to reduce the effect of multiple contributions of bioclimatic variables on the MaxEnt model. Bioclimatic variables with high correlation coefficients ($|r| \geq 0.90$) were removed. Finally, bioclimatic variables were screened based on the jackknife test and correlation analysis.

Table 1. Bioclimatic variables used in the MaxEnt model.

Bioclimatic Variables	Description	Unit
Bio1	Annual mean temperature	°C
Bio2	Mean diurnal range	°C
Bio3	Isothermality	
Bio4	Temperature seasonality	
Bio5	Max temperature of the warmest month	°C
Bio6	Min temperature of the coldest month	°C
Bio7	Temperature annual range	°C
Bio8	Mean temperature of wettest quarter	°C
Bio9	Mean temperature of driest quarter	°C
Bio10	Mean temperature of warmest quarter	°C
Bio11	Mean temperature of coldest quarter	°C
Bio12	Annual precipitation	mm
Bio13	Precipitation of the wettest month	mm
Bio14	Precipitation of the driest month	mm
Bio15	Precipitation seasonality	
Bio16	Precipitation of the wettest quarter	mm
Bio17	Precipitation of the driest quarter	mm
Bio18	Precipitation of the warmest quarter	mm
Bio19	Precipitation of the coldest quarter	mm

2.3. Model Settings and Evaluation

The distribution points of sesame and bioclimatic variables were imported into the MaxEnt (version 3.4.4) software to predict the climatic suitability. The model parameters were set to a convergence threshold of 10^{-5}, a maximum number of background points of 5000, and a cloglog output format. Seventy-five percent of the bioclimatic variables were randomly selected as training data to establish the basic model parameters. The remaining 25% used as test data to assess the model's applicability [28]. For each subsample type, we ran 10 replicates and averaged the results to reduce model uncertainty [29]. To reduce the model overfitting, various combinations were tested to identify the optimal model parameters. The regularization level of the MaxEnt model comprises two parameters: the regularization multiplier (RM) and the feature combination (FC). The RM was set from 1.0 to 2.5 with 0.5 intervals. Five sets of FC are set up for optimizing the model parameters (LH: linear and hinge; LQ: linear and quadratic; LQH: linear, quadratic, and hinge; LQPT: linear, quadratic, product, and threshold; LQHPT: linear, quadratic, hinge, product, and threshold) [30]. The test sensitivity at 0% and 10% training omission rates (ORs) was utilized to select the best model. A test omission rate closer to 0 at 0% and to 0.100 at 10% indicated a higher-ranking model [31]. The performance of the MaxEnt model was evaluated by the receiver operating curve (ROC), which plots sensitivity versus (1–specificity) [32,33]. The area under the curve (AUC) is a useful threshold-independent metric for assessing a model's ability to differentiate between presence and absence, with values ranging from 0 to 1. An AUC value below 0.50 means that the simulation result was worse than those simulated by a random model, while a value close to 1.0 means that the model performs better.

2.4. Reclassifying Suitable Areas and Assessing Bioclimatic Variables

The climatically suitable areas of sesame in China were output by the MaxEnt model. ArcGIS 10.8 software was used for spatial mapping of suitability for both present and future climate scenarios. Based on the existence probability (P) produced by the model, the natural break point classification method (Jenks) was applied to categorize the suitable areas: the highly suitable areas (0.8–1.0), the moderately suitable areas (0.5–0.8), the lowly suitable areas (0.2–0.5), and the unsuitable areas (0.0–0.2), as shown in Table 2. The distribution map of sesame in China was created using the reclassification function in ArcGIS, and

the pixel count for various suitable areas was determined through the "attribute–symbol system–unique value" method to calculate the area of suitable areas.

Table 2. Suitability assessment for sesame in China.

Class of Suitability	Existence Probability
Highly suitable	0.8–1.0
Moderately suitable	0.5–0.8
Lowly suitable	0.2–0.5
Unsuitable	0.0–0.2

By using the "Quick Reclassify to Binary" tool in SDMTools in ArcGIS 10.8 [34], areas with an existence probability higher than 0.2 are classified as potentially suitable areas, and areas with an existence probability less than 0.2 are classified as non-potentially suitable areas according to the output results of the MaxEnt model. We finally obtained a raster file with only potentially suitable areas and non-potentially suitable areas. The changes in potentially suitable areas for sesame during different periods were calculated using the "Distribution Change Between Binary SDMs" tool in SDMTools, and the values were defined as 0 for unfit, –1 for expansion, 1 for unchanged, and 2 for contraction [35], and the area of potentially suitable areas in different periods was calculated.

3. Results

3.1. Major Bioclimatic Variable Affecting Sesame Cultivation Distribution

The result of the jackknife test showed that the contribution rates of the max temperature of the warmest month, annual precipitation, and precipitation of the driest month are 21.5%, 12.5%, and 11.3%, respectively (Table 3), indicating that these variables offer more meaningful information to the modeling process. From the correlation analysis of the 13 bioclimatic variables, we removed five highly correlated variables and retained eight variables for this model.

Table 3. Relative contributions of bioclimatic variables in the MaxEnt model.

Bioclimatic Variables	Percent Contribution	Permutation Importance
Max temperature of the warmest month	21.5	11.6
Annual precipitation	13.5	26.4
Precipitation of the driest month	11.3	16
Precipitation of the wettest month	11.2	2.2
Precipitation of the driest quarter	10.8	3.3
Mean temperature of the warmest quarter	6.8	1.1
Temperature seasonality	5.7	4.8
Mean temperature of the wettest quarter	4.7	7.8
Temperature annual range	4.1	3.4
Isothermality	2.7	1.2
Annual mean temperature	1.8	0.3
Mean diurnal range	1.6	0.7
Precipitation seasonality	1.4	9.6
Precipitation of the coldest quarter	0.8	3.5
Mean temperature of driest quarter	0.6	1.9
Min temperature of the coldest month	0.5	0.2
Precipitation of the wettest quarter	0.5	0.5
Precipitation of the warmest quarter	0.2	5.3
Mean temperature of the coldest quarter	0.1	0.2

As shown in Figure 2, the maximum temperature of the warmest month had the highest effect on the climatic suitability for sesame within each category of bioclimatic variables, followed by annual mean temperature, annual precipitation, mean diurnal range, precipitation of driest month, isothermality, precipitation seasonality, and temperature seasonality (Figure 2).
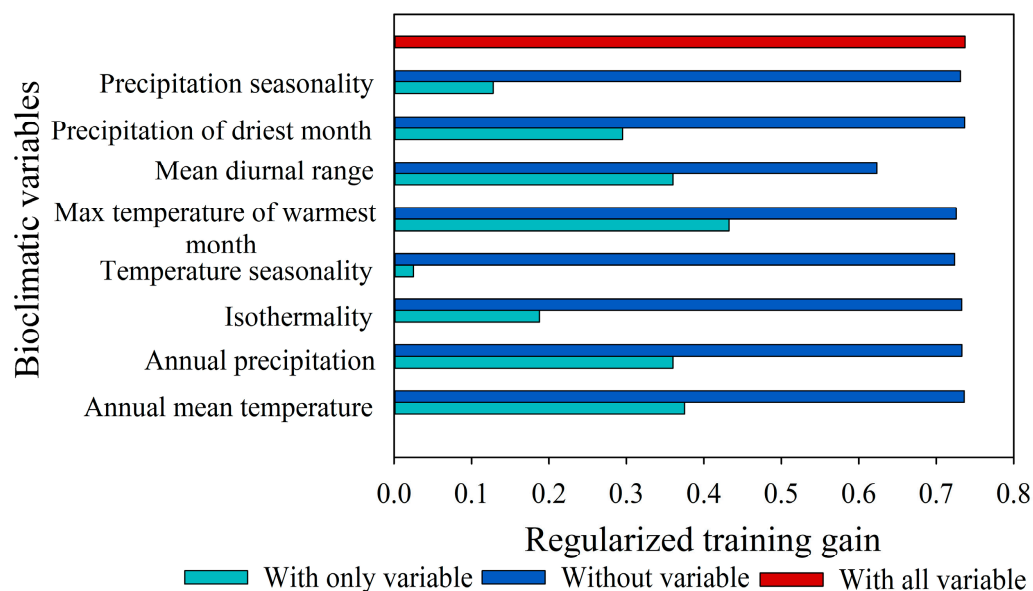

Figure 2. Results of jackknife test of bioclimatic variables for the suitability of sesame.

We selected the top five bioclimatic variables with high contribution rates to judge the relationship between distribution probability and bioclimatic variables (Figure 3). It was assumed that if the existence probability of sesame exceeded 0.5, the corresponding bioclimatic variables were suitable for plant growth [36].

As shown in Figure 3, the probability was less than 0.5 when the max temperature of the warmest month was less than 29.94 °C and greater than 34.08 °C. The probability was the highest at 0.667 when the max temperature of the warmest month was 34.08 °C. So the optimum value of the max temperature of the warmest month was 29.94–34.08 °C. The probability was less than 0.5 when the annual mean temperature was less than 13.60 °C. The probability was the highest at 0.759 when the annual mean temperature was 29.90 °C. So the optimum value was 13.60–29.90 °C. The probability was less than 0.5 when the annual precipitation was less than 814.20 mm. The probability was the highest at 0.678 when the annual precipitation was 1801.28 mm. So the optimum value was 814.20–1801.28 mm. The probability was less than 0.5 when the mean diurnal range was greater than 10.32 °C. The probability was the highest at 0.687 when the mean diurnal range was 2.66–4.07 °C. So the optimum value was 2.66–10.32 °C. The probability was less than 0.5 when the precipitation of the driest month was less than 11.50 mm. The probability was the highest at 0.851 when the precipitation of the driest month was 116.64–117.57 mm. So the optimum value was 11.50–212.30 mm.
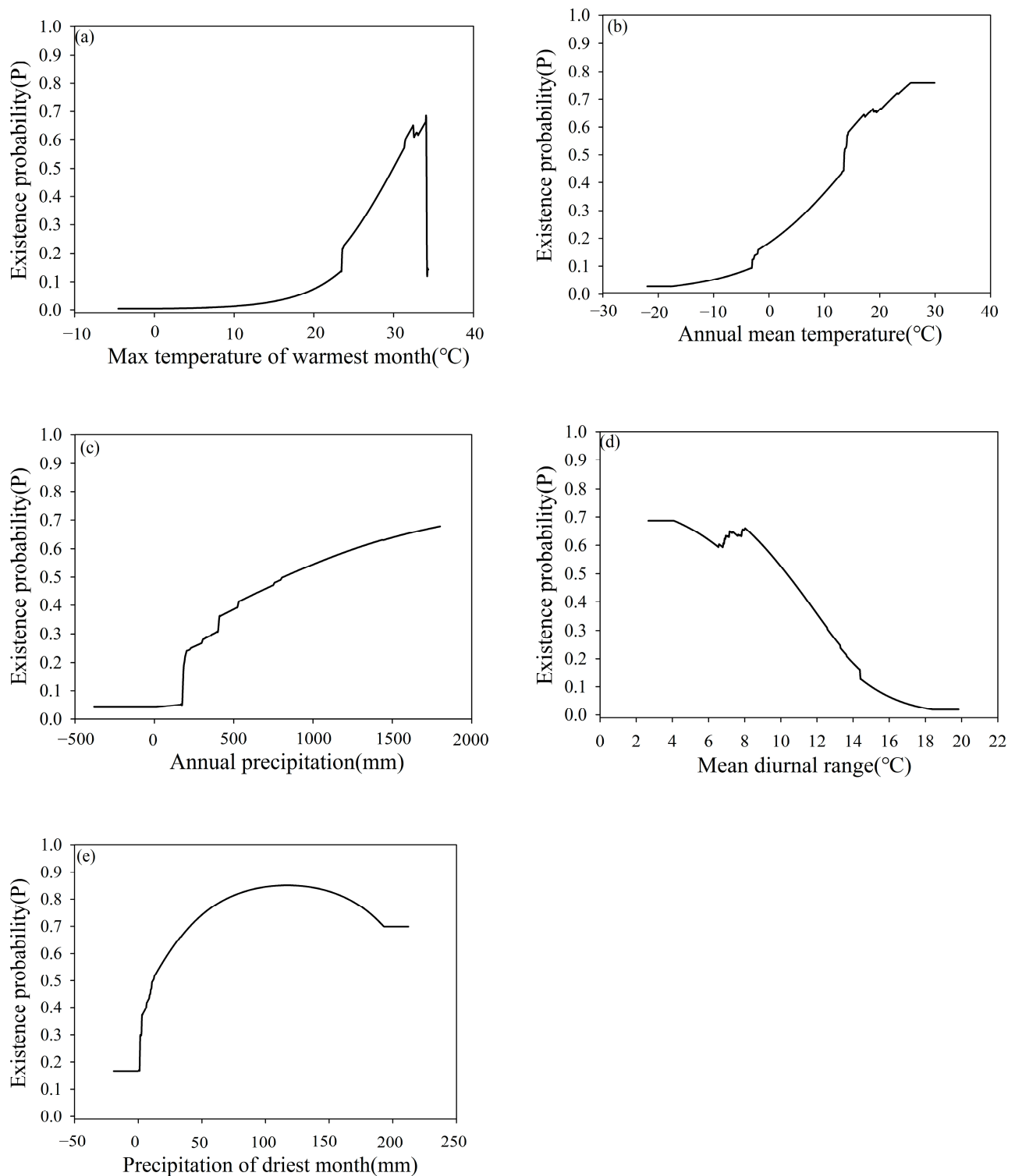
Figure 3. Responses of the five major bioclimatic variables to sesame: (**a**) max temperature of warmest month, (**b**) annual mean temperature, (**c**) annual precipitation, (**d**) mean diurnal range, and (**e**) precipitation of driest month.

3.2. Model Calibration and Performance

The models with different settings achieved low test omission rates, ranging from 0.004 to 0.059 at a 0% training omission rate and from 0.095 to 0.127 at a 10% training omission rate (Table 4). Both results were more aligned with the expected value when the test omission rates at 0% and 10% were 0.004 and 0.095, and the corresponding AUC test

was 0.841, showing a high prediction accuracy. Therefore, the linear, quadratic, product, threshold, and RM = 2.0 were chosen as the best model parameters to reduce overfitting.

Table 4. Performance of the MaxEnt model with various parameter settings.

Setting		OR		$AUC_{test} \pm SD$
RM	**FC**	**0%**	**10%**	
1	LH	0.029	0.184	0.810 ± 0.023
1.5	LH	0.013	0.109	0.827 ± 0.021
2	LH	0.013	0.113	0.831 ± 0.021
2.5	LH	0.009	0.138	0.813 ± 0.022
1	LQ	0.059	0.127	0.816 ± 0.023
1.5	LQ	0.007	0.102	0.817 ± 0.023
2	LQ	0.009	0.127	0.807 ± 0.024
2.5	LQ	0.018	0.116	0.811 ± 0.024
1	LQH	0.018	0.179	0.812 ± 0.023
1.5	LQH	0.016	0.161	0.823 ± 0.022
2	LQH	0.009	0.146	0.824 ± 0.022
2.5	LQH	0.007	0.102	0.829 ± 0.021
1	LQPT	0.025	0.216	0.817 ± 0.023
1.5	LQPT	0.016	0.143	0.832 ± 0.022
2	LQPT	0.004	0.095	0.841 ± 0.020
2.5	LQPT	0.011	0.138	0.828 ± 0.022
1	LQHPT	0.016	0.198	0.822 ± 0.022
1.5	LQHPT	0.029	0.175	0.824 ± 0.023
2	LQHPT	0.009	0.132	0.826 ± 0.021
2.5	LQHPT	0.009	0.166	0.816 ± 0.022

SD is the standard deviation. AUC_{test} refers to the area under the receiver operating characteristic curve calculated using test data.

The screened eight bioclimatic variables were imported into the MaxEnt model with the selected parameters. The average AUC value of the test sets was 0.841, indicating that the MaxEnt model has high prediction accuracy, and is reliable for predicting the suitable areas of sesame planting (Figure 4).
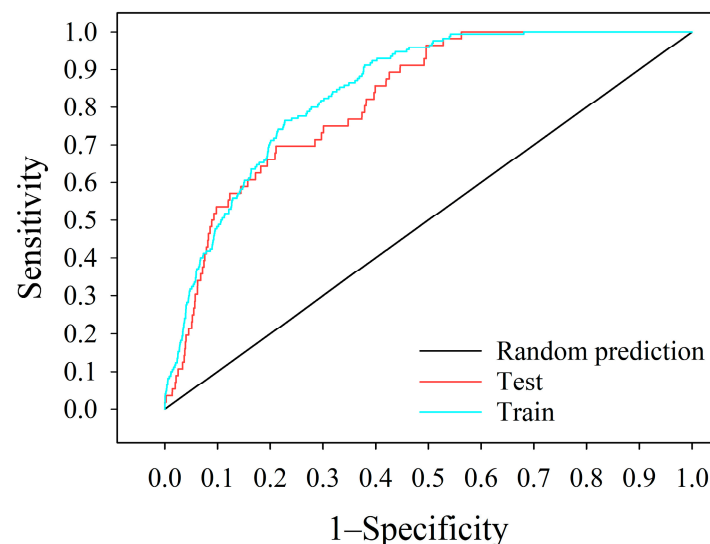

Figure 4. Receiver operating curve with the corresponding area under the curve.

3.3. Spatial Distribution of Suitable Areas for Sesame Under Current Climate Scenario

Figure 5 shows that under the current scenario, the suitable areas (highly suitable areas, moderately suitable areas, and lowly suitable areas) of sesame were widely distributed

in China, from south (Hainan) to north (Heilongjiang) and from east (Yellow Sea) to west (Tibet). The area of suitable areas was 481.95×10^4 km^2, accounting for 49.96% of the total land area in China. The area of highly suitable areas was 64.51×10^4 km^2, accounting for 6.69%, and mainly located in southern central Henan, eastern central Hubei, northern central Anhui, northern central Jiangxi, and eastern central Hunan. The area of moderately suitable areas was 168.16×10^4 km^2, accounting for 17.45%, and concentrated in northeast Henan, eastern Sichuan, most parts of Hebei, Shandong, Jiangsu, Fujian, Guangdong, Guangxi, and Hainan, small parts of Heilongjiang, Jilin, Liaoning, Yunnan, and Xinjiang. The area of lowly suitable areas was 249.28×10^4 km^2, accounting for 25.82%, primarily distributed in eastern Sichuan, most parts of Guizhou, Shaanxi, Shanxi, Ningxia, Heilongjiang, Jilin, Liaoning, Yunnan, and Inner Mongolia, small parts of Gansu and Shandong.
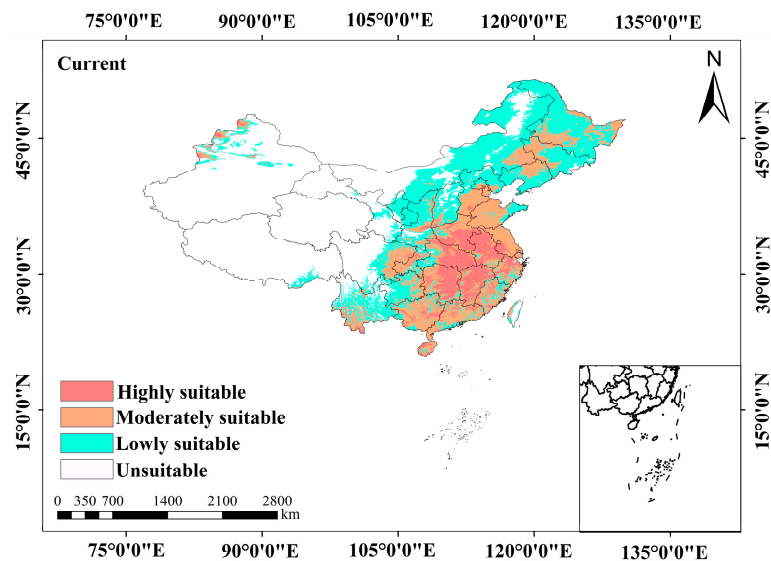
Figure 5. Potentially suitable areas for sesame under the current climate scenario in China.

3.4. Spatial Distribution of Suitable Areas for Sesame Under Future Climate Scenarios

Figure 6 shows that the distribution of suitable areas had the same trend under the future climate scenarios compared with the current climate scenario. The area of total suitable areas ranged from 448.31×10^4 km^2 to 477.49×10^4 km^2, accounting for 46.51–49.54% of China's total land area. The area of highly suitable areas, moderately suitable areas, lowly suitable areas, and unsuitable areas ranged from 60.05×10^4–71.92×10^4 km^2, 129.43×10^4–167.65×10^4 km^2, 237.17×10^4–270.88×10^4 km^2, 486.39×10^4–515.56×10^4 km^2, respectively.

No significant difference in the distribution of suitable areas under future climate scenarios compared to the current climate scenario. Furthermore, under SSP126 in 2021–2040, 2041–2060, 2061–2080, and 2081–2100, the area of highly suitable areas accounted for 6.84%, 6.26%, 6.97%, and 6.79% of China's total land area, as well as accounting for 6.83%, 6.75%, 6.70%, and 7.04% under SSP245, accounting for 6.23%, 6.75%, 7.06%, and 7.46% under SSP370, accounting for 6.73%, 6.70%, 6.85%, and 6.58% under SSP585.

The area of moderately suitable areas accounted for 13.84%, 17.39%, 13.43%, and 13.87% under SSP126 in 2021–2040, 2041–2060, 2061–2080, 2081–2100, as well as accounting for 14.71%, 13.74%, 14.32%, and 15.65% under SSP245, accounting for 15.05%, 14.68%, 14.37%, and 14.27% under SSP370, accounting for 16.15%, 15.90%, 14.03%, 16.04% under SSP585. The area of lowly suitable areas and unsuitable areas accounted for 24.61–28.10% and 50.46–53.49% under future climate scenarios, respectively.

Figure 6. Potentially suitable areas for sesame under future climate scenarios in China.

As shown in Table 5, under SSP126, the area of highly suitable areas decreased by 6.43% during 2041–2060 and increased by 2.27%, 4.13%, and 1.42% during 2021–2040, 2061–2080, and 2081–2100. The area of highly suitable areas during four periods increased by 2.09%, 0.85%, 0.10%, and 5.14% under SSP245. Under SSP370, the area of highly suitable areas increased by 0.78%, 5.47%, and 11.48% during 2041–2060, 2061–2080, and 2081–2100 and decreased by 6.92% during 2021–2040. Under SSP585, the area of highly suitable areas increased by 0.60%, 0.16%, and 2.39% during 2021–2040, 2041–2060, and 2061–2080 and decreased by 1.73% during 2081–2100.

The area of moderately suitable areas during four periods decreased by 20.67%, 0.31%, 23.03%, and 20.49% under SSP126, as well as decreasing by 15.71%, 21.24%, 17.90%, and 10.29% under SSP245, decreasing by 13.74%, 15.89%, 17.61%, and 18.19% under SSP370, respectively, decreasing by 7.42%, 8.85%, 19.61%, and 8.05% under SSP585.

The increased highly suitable areas were mainly concentrated in northern Henan. The decreased moderately suitable areas for sesame were mainly distributed in Heilongjiang, Jilin, and Liaoning.

Table 5. The difference of suitable areas under current and future climate scenarios.

Scenarios	Periods	Predicted Area (10^4 km^2)				Comparison with Current Distribution (%)			
		Unsuitable Areas	Lowly Suitable Areas	Moderately Suitable Areas	Highly Suitable Areas	Unsuitable Areas	Lowly Suitable Areas	Moderately Suitable Areas	Highly Suitable Areas
Current	1970–2000	481.92	249.28	168.16	64.51				
SSP126	2021–2040	499.96	264.54	133.40	65.97	3.74	6.12	−20.67	2.27
	2041–2060	486.39	249.47	167.65	60.36	0.93	0.08	−0.31	−6.43
	2061–2080	496.39	270.88	129.43	67.17	3.00	8.67	−23.03	4.13
	2081–2100	510.36	254.38	133.70	65.43	5.90	2.05	−20.49	1.42
SSP245	2021–2040	510.34	245.93	141.74	65.86	5.90	−1.34	−15.71	2.09
	2041–2060	504.78	261.59	132.44	65.06	4.74	4.94	−21.24	0.85
	2061–2080	500.36	260.87	138.06	64.58	3.83	4.65	−17.90	0.10
	2081–2100	508.02	237.17	150.86	67.82	5.42	−4.86	−10.29	5.14
SSP370	2021–2040	515.56	243.21	145.06	60.05	6.98	−2.43	−13.74	−6.92
	2041–2060	501.32	256.09	141.45	65.01	4.03	2.70	−15.89	0.78
	2061–2080	504.40	252.89	138.54	68.04	4.66	1.45	−17.61	5.47
	2081–2100	488.10	266.28	137.57	71.92	1.28	6.82	−18.19	11.48
SSP585	2021–2040	491.86	251.42	155.68	64.90	2.06	0.86	−7.42	0.60
	2041–2060	503.26	242.72	153.28	64.61	4.43	−2.63	−8.85	0.16
	2061–2080	495.23	267.40	135.19	66.05	2.76	7.27	−19.61	2.39
	2081–2100	493.90	251.95	154.63	63.39	2.49	1.07	−8.05	−1.73

Under the four climate scenarios, the area of unsuitable areas increased, ranging from 0.93% to 6.98%. The area of lowly suitable areas increased, ranging from 0.08% to 8.67%, with the largest increase in 2061–2080 under SSP126, followed by 2081–2100 under SSP370 with 6.82%. In contrast, the area of lowly suitable areas decreased, ranging from 1.34% to 4.86%, with the largest decrease in 2081–2100 under SS245, followed by 2041–2060 under SSP585 with 2.63%.

3.5. Changes in the Spatial Distribution of Suitable Areas for Sesame

The suitable areas under the four future climate scenarios were mainly concentrated in Heilongjiang, Liaoning, Jilin, Beijing, Tianjin, Shandong, Hebei, Henan, Anhui, Hubei, Jiangxi, Hunan, Guangxi, Guangdong, Fujian, Jiangsu, Zhejiang, and most parts of Sichuan, Yunnan, Inner Mongolia, Shanxi, and Shaanxi (Figure 7).

As shown in Table 6, under SSP126, the potential distribution of sesame presented an overall contraction trend in current–2040s, 2060s–2080s, and 2080s–2100s, the area of suitable areas shrank by 2.44%, 1.97%, and 1.96%, comprising 23.56×10^4 km^2, 19.00×10^4 km^2, and 18.86×10^4 km^2, respectively, which mainly concentrated in southeast Inner Mongolia and eastern Yunnan. However, the area of suitable areas in the 2040s–2060s expanded by 20.90×10^4 km^2 (2.17%), which was mainly concentrated in southeast Inner Mongolia.

Under SSP245, the area of suitable areas in the current–2040s and 2080s–2100s shrank by 31.17×10^4 km^2 (3.23%) and 17.80×10^4 km^2 (1.85%), were mainly concentrated in southeast Inner Mongolia and eastern Yunnan. In contrast, the suitable areas of sesame presented an expansion trend in the 2040s–2060s and 2060s–2080s, the area of suitable areas expanded by 1.84% and 0.88%, comprising 17.76×10^4 km^2 and 8.48×10^4 km^2, where mainly concentrated in central Inner Mongolia and eastern Yunnan.

Under SSP370, the potential distribution of sesame presented an overall contraction trend in the current–2040s and 2060s–2080s, the area of suitable areas shrank by 38.74×10^4 km^2 (4.02%) and 10.46×10^4 km^2 (1.09%), respectively, which mainly concentrated in eastern Inner Mongolia, eastern Gansu, and eastern Yunnan. However, the area of suitable areas in the 2040s–2060s and 2080s–2100s expanded by 2.36% and 2.06%, comprising 22.75×10^4 km^2 and 19.85×10^4 km^2, where mainly concentrated in eastern Inner Mongolia, eastern Gansu, and eastern Yunnan.
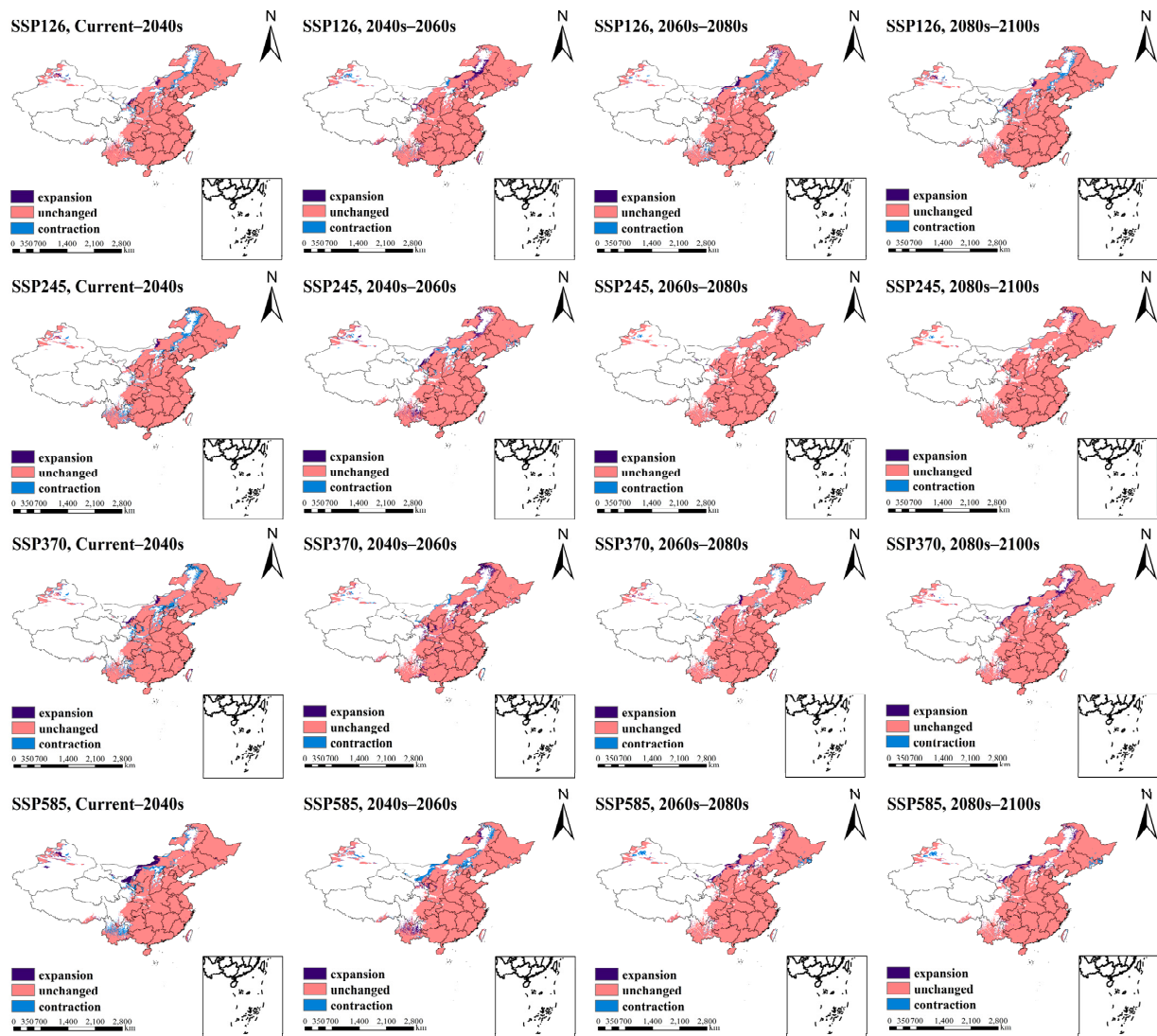
Figure 7. Changes in suitable areas for sesame in different periods.

Table 6. Area of suitable areas for sesame in different periods.

		Current–2040s		2040s–2060s		2060s–2080s		2080s–2100s	
		Area (10^4 km²)	Percent (%)	Area (10^4 km²)	Percent (%)	Area (10^4 km²)	Percent (%)	Area (10^4 km²)	Percent (%)
SSP126	Expansion	5.52	0.57	20.90	2.17	9.01	0.93	4.90	0.51
	Unsuitable	476.40	49.43	479.06	49.70	477.38	49.53	491.49	50.99
	Unchanged	458.39	47.56	456.58	47.37	458.48	47.57	448.62	46.54
	Contraction	23.56	2.44	7.33	0.76	19.00	1.97	18.86	1.96
SSP245	Expansion	2.75	0.29	17.76	1.84	8.48	0.88	10.14	1.05
	Unsuitable	479.17	49.71	492.58	51.10	496.30	51.49	490.22	50.86
	Unchanged	450.78	46.77	441.32	45.79	455.03	47.21	445.71	46.24
	Contraction	31.17	3.23	12.21	1.27	4.06	0.42	17.80	1.85
SSP370	Expansion	5.11	0.53	22.75	2.36	7.38	0.77	19.85	2.06
	Unsuitable	476.81	49.47	492.80	51.13	493.94	51.25	484.55	50.27
	Unchanged	443.21	45.98	439.80	45.63	452.09	46.90	455.92	47.30
	Contraction	38.74	4.02	8.51	0.88	10.46	1.09	3.55	0.37
SSP585	Expansion	16.78	1.74	14.36	1.49	15.98	1.66	12.77	1.33
	Unsuitable	465.14	48.26	477.50	49.54	487.28	50.55	482.45	50.05
	Unchanged	455.23	47.23	446.25	46.30	452.67	46.96	457.20	47.43
	Contraction	26.72	2.77	25.76	2.67	7.95	0.82	11.45	1.19

Under SSP585, the suitable areas of sesame presented an overall contraction trend in the current–2040s and 2040s–2060s, the area of suitable areas shrank by 26.72×10^4 km^2 (2.77%) and 25.76×10^4 km^2 (2.67%), where mainly concentrated in central and eastern Inner Mongolia. In contrast, the suitable areas in 2060s–2080s and 2080s–2100s, respectively, expanded by 1.66% and 1.33%, comprising 15.98×10^4 km^2 and 12.77×10^4 km^2.

4. Discussion

4.1. Effect of Bioclimatic Variables on Geographical Distribution of Sesame

Bioclimatic variables are the main factors that regulate crop growth rate, yield, and geographical distribution. In order to understand the effect of bioclimatic variables on the geographical distribution of sesame, this study analyzed the input variables of MaxEnt model using jackknife test and determined that the max temperature of the warmest month (Bio5) was the critical bioclimatic variable affecting the sesame distribution, followed by annual mean temperature (Bio1), annual precipitation (Bio12), mean diurnal range (Bio2), precipitation of driest month (Bio14), isothermality (Bio3), precipitation seasonality (Bio15), and temperature seasonality (Bio4). Based on the response curve, the probability of sesame distribution and the range of values for each bioclimatic variable are determined. Among these variables, the optimum value range of the annual mean temperature was 13.60–29.90 °C, and the optimal value range of the max temperature of the warmest month was 29.94–34.08 °C. Baath et al. [22] found that the basic temperature limits to fulfill sesame biomass accumulation were 15.7 °C (T$_{min}$), 27.3 °C (T$_{opt}$), and 44.6 °C (T$_{max}$). Sesame was able to flower at medium and high temperatures. However, the yield gradually decreases when the temperature is above 25 °C, and there is no seed yield when the temperature is above 33 °C. In addition, Wang et al. [37] found that long-term temperatures higher than 35 °C will retard growth and delay flowering. Our findings are consistent with previous studies conducted by Baath [22] and Wang [37].

Global warming intensifies the global water cycle, resulting in more extreme precipitation. Sesame is sensitive to waterlogging, and excessive moisture conditions can severely hinder its growth and decrease yield and quality [38]. However, drought at the sowing stage decreases the seedling emergence rate, and persistent drought in the growth stage delays the growth and development of sesame [39]. Our results showed that the sum of the contributions of annual precipitation and precipitation of the driest month was 11.4%, and the optimal range of annual precipitation was 814.20–1801.28 mm, the optimal range of precipitation of the driest month was 11.50–212.30 mm.

4.2. Effect of Climate Change on Geographical Distribution of Sesame

Our results showed that sesame is widely distributed in China, from south (Hainan) to north (Heilongjiang) and from east (Yellow Sea) to west (Tibet). Luo et al. [40] indicated that sesame is widely distributed in China. And the sesame planting areas are mainly concentrated in Henan, Hubei, and Anhui, accounting for about 70% of the total sesame planting areas, followed by Jiangxi, Jiangsu, Shandong, Hunan, Hebei, and other provinces, accounting for about 20% of the total sesame-planting areas. Based on national statistical data from 1985 to 2015, Wang et al. [41] found that the sesame-planting areas in China are mainly concentrated in the Dabie Mountain Range area and northwestern Liaoning. In our study, the highly suitable areas were concentrated in southern central Henan, eastern central Hubei, northern central Anhui, northern central Jiangxi, and eastern central Hunan. The moderately suitable areas were concentrated in northeast Henan, eastern Sichuan, most parts of Hebei, Shandong, Jiangsu, Fujian, Guangdong, Guangxi, and Hainan. In this study, the AUC value of the MaxEnt model was 0.841, and the model predictions were consistent with the actual distribution, indicating that the MaxEnt model is reliable in predicting the distribution of sesame.

Under the future climate scenarios, the contraction rate of suitable areas for sesame is greater than the expansion rate, with a decreasing trend in the suitable areas. The area of unsuitable areas showed an increasing trend. Among the suitable areas, the area of highly

suitable areas and low suitable areas all increased. In contrast, the area of moderately suitable areas decreased, ranging from 0.31% to 23.03%. The decline range in moderately suitable areas was higher than the increase range in highly suitable and lowly suitable areas, resulting in a decrease in suitable areas. This may be because moderately suitable areas are usually closer to crop or ecosystem tolerance thresholds, and small environmental changes may result in significant reductions in moderately suitable areas.

The fifth assessment report of the Intergovernmental Panel on Climate Change (IPCC) points out that the global warming is about 1.5 °C, 1.1–2.6 °C, 1.4–3.1 °C, and 2.6–4.8 °C under different future climate scenarios. In this study, climate warming under different scenarios had different effects on sesame suitability. The area of highly suitable areas increased, ranging from 0.10% to 11.48%, except for 2041–2060 under SSP126, 2021–2040 under SSP370, and 2081–2100 under SSP585. The lowly suitable areas increased, ranging from 0.08% to 8.67% except for 2021–2040 and 2081–2100 under SSP126, 2021–2040 under SSP370, and 2041–2060 under SSP585. The area of highly suitable areas increased significantly under SSP370. The temperature rise of 1.4–3.1 °C is conducive to the spatial expansion of sesame. Therefore, the bioclimatic variables under SSP370 are more favorable for the expansion of suitable areas for sesame in China because increasing temperatures and precipitation are more capable of meeting the climatic demands of sesame in China.

Under the four future climate scenarios, the highly suitable areas for sesame were centered on the five traditional sesame planting areas, including Henan, Anhui, Hubei, Hunan, and Jiangxi, which have a relatively stable distribution pattern. These regions are characterized by favorable climatic conditions, such as adequate precipitation and suitable temperatures. The study showed that no significant migration of the suitable areas was found. In addition, the increased highly suitable areas were mainly located in northern Henan because of the thermophilic habit of sesame, and climate warming promoted the expansion of sesame planting areas. In addition, climate warming led to an increase in precipitation [42]. Sesame is a drought-tolerant and flood-resistant crop [43,44]. Northern Henan has low precipitation throughout the year, and the increased precipitation creates more favorable conditions for sesame growth. The decreased moderately suitable areas were mainly distributed in Liaoning and other northeastern regions due to increased evaporation caused by increasing temperatures. High evaporation led to an increased demand for sesame precipitation, and precipitation in the northeast areas did not meet the demand for sesame growth.

4.3. Suggestions and Potential Limitations

Wang et al. [41] also found that China's sesame production areas have changed slightly in the past 30 years, mainly concentrated in Henan, Anhui, and Hubei. Therefore, when choosing sesame-planting areas, factors such as policy and capital should be first considered, followed by climatic factors. In addition, it is recommended to increase sesame-planting areas in the highly suitable areas and the moderately suitable areas, such as southern central Henan, northeast Henan, eastern central Hubei, northern central Anhui, northern central Jiangxi, eastern central Hunan, eastern Sichuan, Hebei, and Shandong.

This study predicted the potential distribution areas of sesame in China by evaluating the effects of meteorological resources on sesame. However, we did not consider the effects of soil, topography, climate disasters, and bioecological factors. In future research, we will incorporate these additional variables to enhance the prediction accuracy of suitable areas for sesame distribution.

5. Conclusions

This study showed that the crucial bioclimatic variables affecting sesame distribution were max temperature of warmest month, annual mean temperature, annual precipitation, mean diurnal range, precipitation of driest month, isothermality, precipitation seasonality, and temperature seasonality. The suitable areas of sesame distribution changed with meteorological resources. Under the current climate scenario, the area of highly suitable

areas, moderately suitable areas, and lowly suitable areas accounted for 6.69%, 17.45%, and 25.82% of China's total land area, respectively. Compared with the current climate scenario, the suitable areas expanded ranging from 0.29% to 2.36% and contracted ranging from 0.42% to 4.02%, were mainly distributed in eastern Inner Mongolia, eastern Gansu, and eastern Yunnan. Furthermore, the area of highly and lowly suitable areas under future climate scenarios increased by 0.10–11.48% and 0.08–8.67%, while the area of moderately suitable areas decreased by 0.31–23.03%. The suitable areas for sesame cultivation shifted slightly, the area of highly suitable areas in northern Henan increased, the area of moderately suitable areas in Heilongjiang, Jilin, and Liaoning decreased, and the lowly suitable areas in Inner Mongolia decreased. And the bioclimatic variables under SSP370 are more favorable for the expansion of suitable areas for sesame in China under future climate scenarios. Our study offers insights into both current and future suitable areas and supplies an adaptive management strategy for sesame cultivation in China in the face of climate change.

Author Contributions: G.L.: formal analysis, visualization, writing—original draft, and funding acquisition; X.W.: data curation, formal analysis, and writing—original draft; J.Z.: methodology and formal analysis; F.H.: conceptualization and writing—review and editing; H.Z.: data curation and supervision; T.G.: formal analysis and project administration; Y.L. and M.H.: supervision and writing—review and editing. All authors have read and agreed to the published version of the manuscript.

Institutional Review Board Statement: Not applicable.

Data Availability Statement: The data that support the findings of this study are available from the Global Biodiversity Information Facility (https://www.gbif.org/), the China Virtual Herbarium (https://www.cvh.ac.cn/), the China National Specimen Information Infrastructure (https://www.nsii.org.cn), the Data Center for Resource and Environmental Sciences, Chinese Academy of Sciences (https://www.resdc.cn/), and the WorldClim database (http://www.wordclim.org).

Conflicts of Interest: The authors declare no conflicts of interest.

References

1. Eftekhari, M.S. Impacts of climate change on agriculture and horticulture. In *Climate Change: The Social and Scientific Construct*; Springer International Publishing: Cham, Switzerland, 2022; pp. 117–131.
2. Kariyawasam, C.S.; Kumar, L.; Ratnayake, S.S. Invasive Plant Species Establishment and Range Dynamics in Sri Lanka under Climate Change. *Entropy* **2019**, *21*, 571. [CrossRef] [PubMed]
3. Schewe, J.; Heinke, J.; Gerten, D.; Haddeland, I.; Arnell, N.W.; Clark, D.B.; Dankers, R.; Eisner, S.; Fekete, B.M.; Colón-González, F.J.; et al. Multimodel assessment of water scarcity under climate change. *Proc. Natl. Acad. Sci. USA* **2014**, *111*, 3245–3250. [CrossRef] [PubMed]
4. Sun, J.; Cheng, G.W.; Li, W.P. Meta-analysis of relationships between environmental factors and aboveground biomass in the alpine grassland on the Tibetan Plateau. *Biogeosciences* **2013**, *10*, 1707–1715. [CrossRef]
5. Zhang, B.; Cui, L.; Shi, J.; Wei, P. Vegetation Dynamics and Their Response to Climatic Variability in China. *Adv. Meteorol.* **2017**, *1*, 8282353. [CrossRef]
6. He, Q.; Zhou, G. Climate-associated distribution of summer maize in China from 1961 to 2010. *Agric. Ecosyst. Environ.* **2016**, *232*, 326–335. [CrossRef]
7. Duan, J.; Zhou, G. Dynamics of decadal changes in the distribution of double-cropping rice cultivation in China. *Sci. Bull.* **2013**, *58*, 1955–1963. [CrossRef]
8. Piirainen, S.; Lehikoinen, A.; Husby, M.; Kålås, J.A.; Lindström, Å.; Ovaskainen, O. Species distributions models may predict accurately future distributions but poorly how distributions change: A critical perspective on model validation. *Divers. Distrib.* **2023**, *29*, 654–665. [CrossRef]

9. Elith, J.; Ferrier, S.; Huettmann, F.; Leathwick, J. The evaluation strip: A new and robust method for plotting predicted responses from species distribution models. *Ecol. Model.* **2005**, *186*, 280–289. [CrossRef]

10. Elith, J.; Graham, C.H.; Anderson, P.R.; Dudík, M.; Ferrier, S.; Guisan, A.; Hijmans, R.J.; Huettmann, F.; Leathwick, J.R.; Lehmann, A.; et al. Novel methods improve prediction of species' distributions from occurrence data. *Ecography* **2006**, *29*, 129–151. [CrossRef]

11. Guisan, A.; Thuiller, W. Predicting species distribution: Offering more than simple habitat models. *Ecol. Lett.* **2005**, *8*, 993–1009. [CrossRef]

12. de Aguiar, C.V.S.; Alencar, J.B.R.; da Silva Santana, G.; Teles, B.R. Predicting the Potential Global Distribution of Scirtothrips dorsalis (Hood) (Thysanoptera: Thripidae) with Emphasis on the Americas Using an Ecological Niche Model. *Neotrop. Entomol.* **2023**, *52*, 512–520. [CrossRef] [PubMed]

13. Kogo, B.K.; Kumar, L.; Koech, R.; Kariyawasam, C.S. Modelling Climate Suitability for Rainfed Maize Cultivation in Kenya Using a Maximum Entropy (MaxENT) Approach. *Agronomy* **2019**, *9*, 727. [CrossRef]

14. Chen, X.; Dimitrov, N.B.; Meyers, L.A. Uncertainty analysis of species distribution models. *PLoS ONE* **2019**, *14*, e0214190. [CrossRef] [PubMed]

15. Huang, T.; Yang, T.; Wang, K.; Huang, W. Assessing the Current and Future Potential Distribution of Solanum rostratum Dunal in China Using Multisource Remote Sensing Data and Principal Component Analysis. *Remote Sens.* **2024**, *16*, 271. [CrossRef]

16. Parthapratim, K.; Bikas, D.; Manoj, K.; Dipanwita, B. Predicting the impact of climate change on habitat suitability and morphological traits of *Begonia aborensis* Dunn in Northeastern India: An endemic taxon of Indo-Myanmar hotspot. *Braz. J. Bot.* **2023**, *46*, 667–680.

17. Zhang, Y.; Dong, Y.; Huang, W.; Guo, J.; Wang, N.; Ding, X. Extraction and Analysis of Grasshopper Potential Habitat in Hulunbuir Based on the Maximum Entropy Model. *Remote Sens.* **2024**, *16*, 746. [CrossRef]

18. Feng, L.; Wang, H.; Ma, X.; Peng, H.; Shan, J. Modeling the current land suitability and future dynamics of global soybean cultivation under climate change scenarios. *Field Crops Res.* **2021**, *263*, 108069. [CrossRef]

19. Wang, Y.J.; Xie, L.Y.; Zhou, X.Y.; Chen, R.F.; Zhao, G.H.; Zhang, F.G. Prediction of the potentially suitable areas of *Leonurus japonicus* in China based on future climate change using the optimized MaxEnt model. *Ecol. Evol.* **2023**, *13*, e10597. [CrossRef]

20. Pandey, B.B.; Ratnakumar, P.; Usha Kiran, B.; Dudhe, M.Y.; Lakshmi, G.S.; Ramesh, K.; Guhey, A. Identifying Traits Associated with Terminal Drought Tolerance in Sesame (*Sesamum indicum* L.) Genotypes. *Front. Plant Sci.* **2021**, *12*, 739896. [CrossRef]

21. Abebe, D.M.; Mengistie, D.T.; Mekonen, A.A. The influence of climate change on the sesame yield in North Gondar, North Ethiopia: Application Autoregressive Distributed Lag (ARDL) time series model. *BMC Plant Biol.* **2024**, *24*, 506. [CrossRef]

22. Baath, G.S.; Kakani, V.G.; Northup, B.K.; Gowda, P.H.; Rocateli, A.C.; Singh, H. Quantifying and Modeling the Influence of Temperature on Growth and Reproductive Development of Sesame. *J. Plant Growth Regul.* **2022**, *41*, 143–152. [CrossRef]

23. Wang, X.; Zhang, J.; Zhang, J.; Zang, H.; Hu, F.; Gao, T.; Huang, M.; Li, Y.; Li, G. Assessing Changes in Climatic Suitability for Sesame Cultivation in China (1978–2019) Based on Fuzzy Mathematics. *Agronomy* **2024**, *14*, 631. [CrossRef]

24. Moss, R.H.; Edmonds, J.A.; Hibbard, K.A.; Manning, M.R.; Rose, S.K.; Van Vuuren, D.P.; Carter, T.R.; Emori, S.; Kainuma, M.; Kram, T.; et al. The next generation of scenarios for climate change research and assessment. *Nature* **2010**, *463*, 747–756. [CrossRef] [PubMed]

25. Hurtt, G.C.; Chini, L.P.; Frolking, S.; Betts, R.A.; Feddema, J.; Fischer, G.; Fisk, J.P.; Hibbard, K.; Houghton, R.A.; Janetos, A.; et al. Harmonization of land-use scenarios for the period 1500–2100: 600 years of global gridded annual land-use transitions, wood harvest, and resulting secondary lands. *Clim. Change* **2011**, *109*, 117. [CrossRef]

26. Cai, Q.Q.; An, M.T.; Yu, J.H.; Tian, L.; Wu, M.X. Suitable habitat prediction of *Pinus kwangtungensis* in China under climate change. *J. Shaanxi Norm. Univ.* **2024**, *52*, 90–102. (In Chinese)

27. Heikkinen, R.K.; Luoto, M.; Araújo, M.B.; Virkkala, R.; Thuiller, W.; Sykes, M.T. Methods and uncertainties in bioclimatic envelope modelling under climate change. *Prog. Phys. Geogr. Earth Environ.* **2006**, *30*, 751–777. [CrossRef]

28. Singh, K.; McClean, C.J.; Büker, P.; Hartley, S.E.; Hill, J.K. Mapping regional risks from climate change for rainfed rice cultivation in India. *Agric. Syst.* **2017**, *156*, 76–84. [CrossRef]

29. Papier, C.M.; Poulos, H.M.; Kusch, A. Invasive species and carbon flux: The case of invasive beavers (*Castor canadensis*) in riparian Nothofagus forests of Tierra del Fuego, Chile. *Clim. Change* **2019**, *153*, 219–234. [CrossRef]

30. Guevara, L.; Gerstner, B.E.; Kass, J.M.; Anderson, R.P. Toward ecologically realistic predictions of species distributions: A cross-time example from tropical montane cloud forests. *Glob. Change Biol.* **2017**, *24*, 1511–1522. [CrossRef]

31. Wang, C.; Shi, X.; Liu, J.; Zhao, J.; Bo, X.; Chen, F.; Chu, Q. Interdecadal variation of potato climate suitability in China. *Agric. Ecosyst. Environ.* **2021**, *310*, 107293. [CrossRef]

32. Fielding, A.H.; Bell, J.F. A review of methods for the assessment of prediction errors in conservation presence/absence models. *Environ. Conserv.* **1997**, *24*, 38–49. [CrossRef]

33. Hanley, J.A.; McNeil, B.J. The meaning and use of the area under a receiver operating characteristic (ROC) curve. *Radiology* **1982**, *143*, 29–36. [CrossRef] [PubMed]

34. Cong, M.; Xu, Y.; Tang, L.; Yang, W.; Jian, M. Predicting the dynamic distribution of Sphagnum bogs in China under climate change since the last interglacial period. *PLoS ONE* **2020**, *15*, e0230969. [CrossRef]

35. Zhang, Y.B.; Liu, Y.L.; Qin, H.; Meng, Q.X. Prediction on spatial migration of suitable distribution of *Elaeagnus mollis* under climate change conditions in Shanxi Province, China. *Chin. J. Appl. Ecol.* **2019**, *30*, 496–502. (In Chinese)

36. Yan, H.; He, J.; Xu, X.; Yao, X.; Wang, G.; Tang, L.; Feng, L.; Zou, L.; Gu, X.; Qu, Y.; et al. Prediction of Potentially Suitable Distributions of *Codonopsis pilosula* in China Based on an Optimized MaxEnt Model. *Front. Ecol. Evol.* **2021**, *9*, 773396. [CrossRef]
37. Wang, X.L.; Tu, Y.; Gu, Z.Q. Comparative study of temperature illumination and water conditions in growing period of autumn sesame and summer in Jianghan Plain. *Chin. J. Oil Crop Sci.* **2002**, *24*, 55–58. (In Chinese)
38. Habibullah, M.; Sarkar, S.; Islam, M.M.; Ahmed, K.U.; Rahman, M.Z.; Awad, M.F.; ElSayed, A.I.; Mansour, E.; Hossain, M.S. Assessing the Response of Diverse Sesame Genotypes to Waterlogging Durations at Different Plant Growth Stages. *Plants* **2021**, *10*, 2294. [CrossRef]
39. Baghery, M.A.; Kazemitabar, S.K.; Dehestani, A.; Mehrabanjoubani, P. Sesame (*Sesamum indicum* L.) response to drought stress: Susceptible and tolerant genotypes exhibit different physiological, biochemical, and molecular response patterns. *Physiol. Mol. Biol. Plants* **2023**, *29*, 1353–1369. [CrossRef]
40. Luo, S.B.; Zhang, X.R.; Wang, Q.; Wang, L.H.; Tang, H.F.; Xu, Y.H.; Cheng, G.W.; Li, Y. Exploration of the development of China's sesame industry in the new era. *Anhui Agric. Sci. Bull.* **2019**, *25*, 47–49+61. (In Chinese)
41. Wang, J.; Fu, M.Q.; Sun, Y.; Liu, B.; Wang, X.H.; Chen, F. Spatio-temporal evolution of sesame production in county-level areas of China during 1985–2015. *J. China Agric. Univ.* **2020**, *25*, 203–213. (In Chinese)
42. Shirazi, S.Z.; Mei, X.R.; Liu, B.C.; Liu, Y. Assessing the impact of climate change in the wheat–maize cropping system across the Huang–Huai–Hai Plain under future climate scenarios. *J. Water Clim. Change* **2022**, *13*, 2847–2871. [CrossRef]
43. Harfi, M.E.; Hanine, H.; Rizki, H.; Latrache, H.; Nabloussi, A. Effect of drought and salt stresses on germination and early seedling growth of different color-seeds of sesame (*Sesamum indicum*). *Int. J. Agric. Biol.* **2016**, *18*, 1088–1094. [CrossRef]
44. Dossa, K.; Li, D.; Wang, L.; Zheng, X.; Yu, J.; Wei, X.; Fonceka, D.; Diouf, D.; Liao, B.; Cisse, N.; et al. Dynamic transcriptome landscape of sesame (*Sesamum indicum* L.) under progressive drought and after rewatering. *Genom. Data* **2017**, *11*, 122–124. [CrossRef] [PubMed]